Combustion Behavior and Quantity Distance Siting

by
Josephine Covino;
Department of Defense Explosives Safety Board, Alexandria, Virginia

Cynthia P. Romo and Jeffrey W. Phillips;
Naval Air Warfare Center Weapons Division, China Lake, California

Alice I. Atwood and Thomas L. Boggs;
Naval Systems Incorporated, Ridgecrest, California

Key Words: Explosives Safety Separation Distance, Quantity Distance, Siting for Combustion Hazards, Burning Rate, Hazard Divisions 1.3 and 1.4, Deflagration, Detonation

Abstract
The paper examines the relationship between combustion behavior and its impact on quantity distance (QD) siting criteria. A series of combustion tests in concrete structures is being studied in order to further understand the hazard response of Hazard Division (HD) 1.3 systems to combustion-driven stimuli. The explosives safety separation distances (ESSDs) or QD siting will be explored as it relates to reaction violence, structural debris (secondary fragments), and pressurization effects. Modified thermal criteria will be presented and discussed. The paper will also identify some of the key parameters in guiding future research in this area.

Introduction
The paper summarizes the current United States (U.S.) Department of Defense Explosives Safety Board (DDESB) siting criteria improvement program for HD 1.3 materials. The siting criteria for HD 1.3 explosives and munition systems is inadequate and, as a result, the DDESB has initiated the thermally driven hazards and siting improvement program.

The Department of Defense Manual (DODM) 6055.09-M [1] is the guiding document that governs the explosives safety siting criteria of all U.S. Department of Defense (DoD) entities. The Allied Ammunition Storage and Transport Publication 1 (AASTP-1) [2] governs the explosives safety siting criteria for North Atlantic Treaty Organization (NATO) operations. Van der Voot et al. [3] provided a comprehensive summary of how the QD tables were determined. Both standards are based on a long history of accidental explosions and many tests where the initiation mechanism was a detonation. Very few experiments have been conducted where the initiation is by ignition and possible pressurization of the structure. The DDESB has recognized that the HD 1.3 criteria presented in both national and international standards does not represent the hazards associated with fire–initiated, or combustion, reactions [4,5,6]. The ignition and combustion properties of HD 1.3 systems and their influence on the thermally driven hazard threat are key parameters in determining the explosives safety QD (or ESSD) for siting operations and processes where fire is the primary hazard. How these parameters influence the structural breakup is of interest to the explosives safety community for siting facilities.

The surface area of the energetic material and its ease of ignition play a strong role in the pressurization rate and subsequent violence of reaction for HD 1.3 systems. Combustion-driven hazard threats exist throughout the entire life cycle of an energetic material or item, ranging from materiel synthesis in research and development, technology maturation, production, deployment operations, support and ultimately disposal [7]. Combustion-driven hazards can occur in all energetic materials and weapon systems. A simplified view of the risk associated with an explosive or munitions event is given in Figure 1, which shows a stimulus (thermal in this case) being introduced to a sample (weapon system) with contributions from the environment to drive a reaction response.

An example of varying responses would be the high surface area of a granular gun propellant versus that of a large solid rocket propellant, stored in an earth-covered magazine or reinforced concrete structure (high confinement) compared to the same system in an International Organization for Standardization (ISO) container. Romo et al. [8] summarize the influence of combustion properties on the hazards potential of HD 1.3 systems. Combustion events are relatively long duration when compared to detonation events (seconds versus milliseconds). These differences can lead to very different response, reaction violence, structural effects, and, in some cases, alter the mechanism and severity of an explosion response.

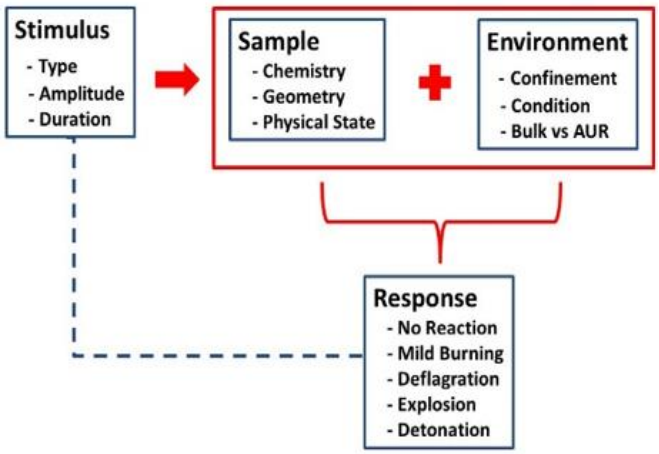

Figure 1. Simplified View of Risk Associated With Combustion-Driven Events [8].

The energy content and physical state of the system play a major role in its response to a specific stimulus. In risk terminology, the risk associated with an explosive event is the probability of the event times the consequence times the exposure time (Equation 1) [5]. The P_e is defined as the probability that an explosives mishap will occur at a potential explosion site (PES) in a year. The $P_{f|e}$ is defined as the probability of fatality given an explosives event and the presence of a person. The E_p is defined as the exposure of one person (as a fraction of a year) to a PES on an annual basis.

$$Risk = Probability\ of\ Event \times Consequences \times Exposure$$
$$\text{Or,} \qquad (1)$$
$$Risk = P_f = P_e \times P_{f|e} \times E_p$$

Boggs et al. [4] presented a review of mishaps from the beginning of the 20th century to March 2012. This review provided an understanding of the predominant hazard encountered by explosives and munitions throughout their life cycle. Over 75% of the mishaps studied had fire as the primary initiation hazard, not explosions or detonations. Often the fires burned for a significant time before either extinguishing or transitioning to an explosion or detonation. Decomposition and self-heating of the energetic from stabilizer depletion or ingredient incompatibility could generate an internal thermal stimulus. The hazard may also be applied externally (an adjacent fire, electrical malfunction, or transportation collision). The response of an item can vary from no reaction to burning, deflagration, explosion, and/or detonation.

The focus of the U.S. Insensitive Munitions (IM) Program is to reduce or eliminate the probability of a detonation and accept a burning reaction [9]. Although IM have been proved very useful in theater, burning reactions of these systems may be more problematic and will likely increase in frequency. Future studies should include a more comprehensive understanding of the contribution and thermal behavior of current and future energetic materials in order to assess the thermal hazards, improve hazard classification methodologies, and redefine siting criteria.

Hazard Classification and Current Siting Criteria in DODM 6055.09-M

Hazard classification addresses threats and conditions for transportation and storage configurations only; it does not consider operational hazard threats [10]. Table 1 summarizes the hazard classification definitions for ammunition and explosives. In the National Fire Protection Association (NFPA) 495-Explosives Material code, conditions, such as those listed in Table 2, are not considered when determining hazard classification [11]. The NFPA 495 document further recommends that a process hazard analysis be conducted at all stages of a munition life cycle since some of these hazards are more prevalent during some parts of the life cycle.

Table 1. Class 1 Hazard Divisions [10].

Hazard Division	Hazard Type
1.1	Mass explosion
1.2.x	Non-mass explosion, fragment producing
1.3	Mass fire, minor blast or fragment
1.4	Moderate fire, no significant blast or fragment
1.5	Explosive substance, very insensitive (with mass explosion hazard)
1.6	Explosive article, extremely insensitive (no mass explosion hazard)

Table 2. Hazards Not Considered in Classification [11].

Electrostatic and electromagnetic influence
Rough handling and vibration
Effects of exposure to hot or cold environments
Mechanical defects
Solar radiation
Temperature shock
Abnormal functioning
Combat exposure

HD 1.3 covers a broad range of munitions, from small grenades and gun propellants, to large diameter solid rocket motors [4]. Propellants and explosives are energetic materials found in missile motors, bombs, and warheads, as well as in bulk. The materials can burn, explode, and/or detonate either on purpose or by accident. However, the initiation mechanism for these materials is usually a thermally driven one possibly followed by deflagration, delayed explosion, or detonation. Accidents with these energetic systems can occur during manufacture, transportation, storage, and operational use. One way to protect personnel and facilities from the risk and consequences of accidents caused by inadvertent reaction of these energetic systems is to provide separation distances between PESs and exposed sites whether they are inhabited buildings, public roadways, or processing buildings.

The methods for QD or ESSD, for the U.S. DoD and NATO are described in detail in References [1] and [2], respectively. These methods (predominantly tables and equations) are largely based on the relationship

$$D = kW^{1/3} \tag{2}$$

Equation (2) defines the distance (D) as equal to the safety weighted factor (k) times the cube root of the energetic weight (W). D is often referred to as the QD (ESSD) for the given weight of energetic material. ESSD or QD are currently determined for the various HDs, with emphasis on HD 1.1. Most of the methods used to evaluate QD for a given energetic material are based on the assumption that the worst-case reaction is detonation, and that the less violent phenomena can be estimated by a simple adjustment (reduction) of the k factor used. However, combustion phenomena do not scale by weight and thus finding a simple relationship may be difficult. Combustion experiments with HD 1.3 gun propellant in concrete structures have been performed to examine the separation distances calculated by such weight based approach for an HD 1.3 systems [5,6,8].

Figure 2 summarizes the QD tables in graphic form presented in DODM 6055.09-M [1]. The data are plotted as open inhabited building distances (IBDs) in meters versus net explosives weight for quantity distance (NEWQD) in kilograms (kg). The graph also summarizes the IBD values from calculated and measured fireball distances in the open and at initial structural breakup. Most of the fireball radius data are scattered in numerous, difficult-to-find reports summarizing detonation tests. Furthermore, trying to understand how these fireball data were measured has proven to be even more difficult.

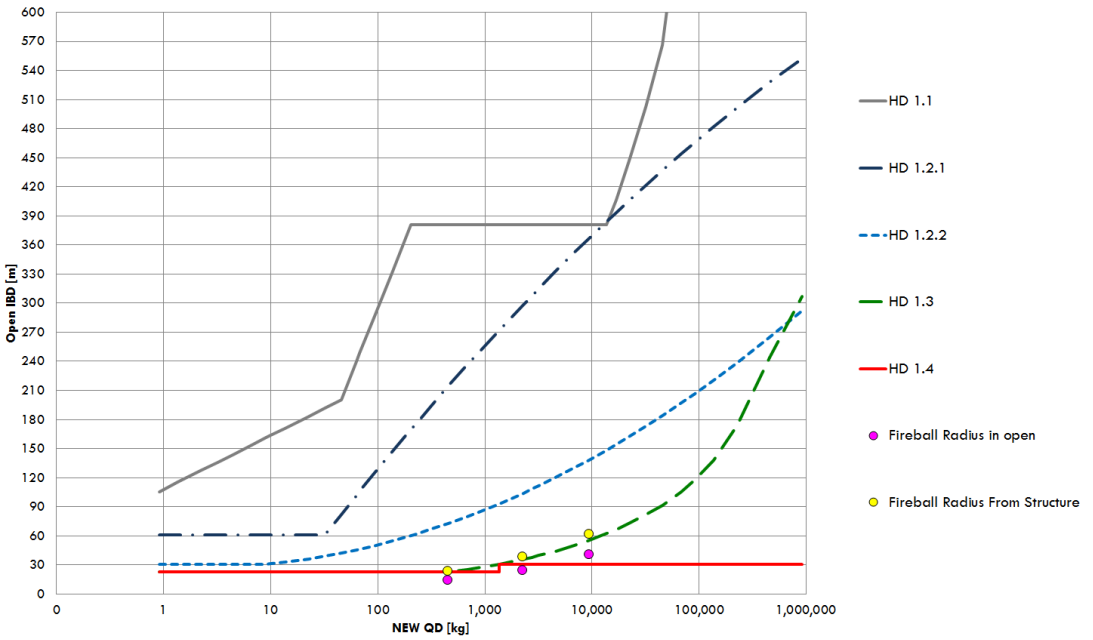

Figure 2. Graph of Open IBD Versus NEWQD.

Figure 3 [12] shows a summary of available fireball radius data obtained via the NATO Program Office for Munitions Safety Information and Analysis Center (MSIAC). The data presented in the figure showed that the HD 1.3 QD tables may be derived from the average of experimental measurements of fireball radii gathered during detonation testing of many different energetic materials and systems. The distances reported are at different test weights; the range of each line in the figure is meant to illustrate the weights of the actual test range. For example, in the case of the rocket propellant charge (Sophy orange line), testing was conducted in the 100 to 60,000 kg weight region. The data are roughly bound by the black dashed line, labeled slow combustion $D = 1{*}W^{1/3}$, and the gray dashed line, labeled detonation and rapid combustion $D = 4{*}W^{1/3}$. It should be noted that the current HD 1.3 tables in DODM 6055.09-M use a safety factor k of 8 for (IBD, and a safety factor k of 5 for interline distances (ILDs). The values reported are at higher heat flux than required in the DODM 6055.09-M. The fireball radii vary significantly based on the combustion characteristics of the specific energetic. These lines represent where the detonation fireball is first observed. Fireball radii data from detonation in structures and in the open are averaged and have a large variation. Survival rate for exposed personnel at this radius is zero. Furthermore, the HD 1.3 curve depicts the demarcation for fatality, and not the demarcation for second-degree burns, as advised by the 2012 heat flux update of the DODM 6055.09-M [1].

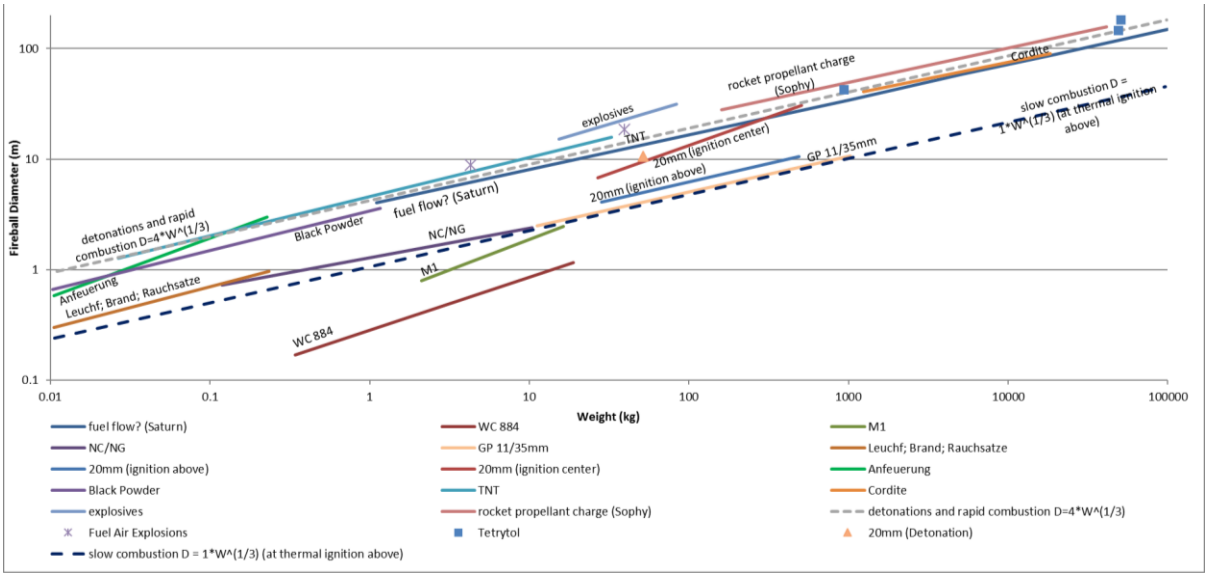

Figure 3. Measured Fire Ball Radius for Different Energetics Materials [10].

The U.S. DoD Joint Service Hazard Classification System (JHCS) database was used to examine items most commonly found in a magazine (largest numbers) and contain the largest amount of energetic material (present largest potential reactivity) [13]. Figures 4 and 5 summarize these data by both number of occurring Navy stock numbers (NSNs) and by net explosive weight (NEW), respectively. The Navy conventional ordnance stockpile consists of items ranging from small arms ammunition to cruise missiles. The ordnance inventory was examined by both number of occurring NSNs, such as with the small ammunition, and NEW, which includes guided missiles. The four hazard class/divisions sorted by NSNs are summarized in Figure 4. The sort by number gives an indication of the kind and type of items that are most likely to be found in a storage magazine. HD 1.4 ordnance makes up the majority (by number), approximately 89%, of the four groups. HD 1.3 makes up approximately 0.6% by number. Combined, the HD 1.3 and HD 1.4 make up about 90%of the items most likely to be found in a storage magazine. The four hazard class/divisions sorted by NEW are summarized in Figure 5. The sort by NEW gives an indication of those items containing the largest amount of energetic material. Ordnance of HD 1.1 makes up the majority (by NEW) of the four group (approximately 79%), with the HD 1.3 making up approximately 11% by weight.

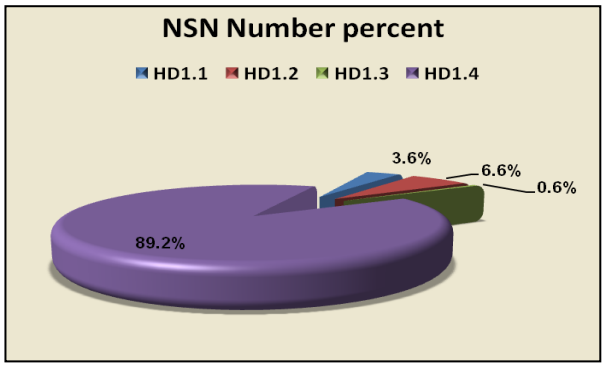

Figure 4. Summary of the Navy Ordnance Inventory by Number of Occurring NSNs.

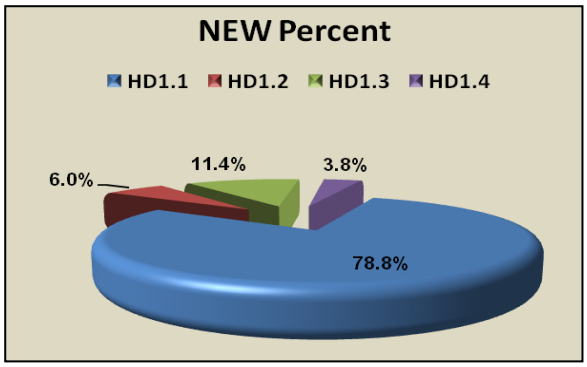

Figure 5. Summary of the Navy Ordnance Inventory by NEW.

In the DoD inventory, the HD 1.3 grouping is often found in mixed storage with HD 1.1 and HD 1.2.x items. Many times the weight that contributes to combustion effects is ignored or significantly reduced when assigned a hazard class. These account for the small number of HD 1.3 items depicted in the two figures. Despite the fact that it appears that most systems are not HD 1.3, in many cases the HD 1.1 and HD1.2.x systems contain HD 1.3 or 1.4 energetic materials or subsystems that have combustion as the predominant hazards (hazard driving the initial energy production process) but have been hazard classified at either HD 1.1 or HD1.2.x at a reduced NEWQD. These weights are not fully represented in the NEWQD (NEWQD is the sum of an adjusted propellant weight plus the warhead weight) values in the JHCS as these quantities are extremely difficult to identify from inventory data. In some cases, this NEWQD may be some experimentally derived and can be a function of how the test was conducted.

The HD 1.3 grouping is further complicated by its broad diversity, ranging from high surface area bulk gun propellant to large rocket motors. Romo et al. [8] provides a comprehensive review of various HD 1.1 and 1.3 substances selected to describe the critical characteristics of these materials relative to the thermal threat. To further complicate the hazard classification assignment of HD 1.3 from fire testing, fragments from the test item (primary fragments) generated from a possible HD 1.3 event require 20 Joules of energy, while the HD 1.1 and 1.2.x require 79 Joules for hazardous fragments [10]. Since the HD 1.3 ESSDs or QDs in the DODM 6055.09-M are based on fireball radius calculations and some spherical fireball (from a detonation) measurements, these distances are not protective from many of the hazards associated with HD 1.3 events. Therefore, providing more inconsistencies in the actual HD 1.3 criteria implemented in the standards.

Subscale Structural Testing

Seven subscale magazine tests were performed at the Naval Air Warfare Center Weapons Division (NAWCWD) with HD 1.3, nitrocellulose (NC)-based gun propellant M1 (formulation detailed in Table 3). The M1 propellant was selected as it represents a sample similar to that found in large numbers of systems in United States Navy (USN) DoD inventory. M1 was also selected in order to compare the results of the current tests with those of previous investigators [14,15]. The Kasun-like [16] structure shown in Figure 6 with the door modified to control vent area was selected as a subscale test structure. This 2 m x 2 m x 2 m structure has been previously used for testing studies of HD 1.1 explosive charges with respect to detonation [17,18]. All seven subscale tests were vented. Tests 1, 3, and 5 were assembled with a 79 cm diameter orifice and did not fail (unchoked condition).

Tests 2, 4, 6, and 7 were assembled with a 39 cm orifice and all failed (choked condition), including Test 7 with the lower loading density. The construction of the structure was modified for Tests 5 through 7 with increased rebar tying the walls and door to the roof of the structure.

Table 3. M1 Propellant Formulation Used in the NAWCWD Tests.

Ingredient	Weight Percent
Nitrocellulose	85.00 +/- 2.00
Dinitrotoluene (DNT)	10.00 +/- 2.00
Dibutylphalate (DBT)	5.00 +/- 1.00
Diphenylamine (DPA)	1.00 +/- 0.10
Lead Carbonate	1.00 +/- 0.20
Potassium Sulfate	1.00 +/- 2.00

Figure 6. Kasun-Like Structure Used for NAWCWD Tests 1-7.

This paper summarizes test results and data presented in other reports and journal articles [4,5,7]. Figures 7 and 8 show the geometries of the two types of M1 propellant tested. Table 4 gives a summary of the loading configuration used in the seven subscale tests as well as the structural response. These combustion tests in subscale concrete structures were performed to evaluate the role of gun propellant surface area and loading density relative to venting, pressurization, plume, and fireball formation. It is recognized that the M1 formulation does not represent the most energetic of HD 1.3 gun propellants.

Romo et al. summarized and detailed combustion hazards as a function of families of propellants and propellant composition [8]. The detailed experimental results for the structural response of M1 in subscale concrete structures have been published and are available in the literature [5,6]. This paper summarizes these data. It further compares the results of the seven tests with respect to combustion effects, and thermal behavior leading to structural failure. Tests 2 and 4 address the differences of configuration/geometry of the M1 grains. Tests 4 and 6 address structural differences. Lastly, Tests 6 and 7 address loading density.

The effect of M1 propellant surface area on closed bomb pressurization rate is illustrated for the smaller, single (1P) and the larger 7 perforation (7P) granules in Figure 9 where the 1P, M1 grains have the larger surface area [4,5,7]. The pressurization rate for the smaller, single (1P) grain is more rapid and the peak is higher. On the other hand, the pressurization rate for the larger seven perforation (7P) granules is slower and the peak not as sharp.

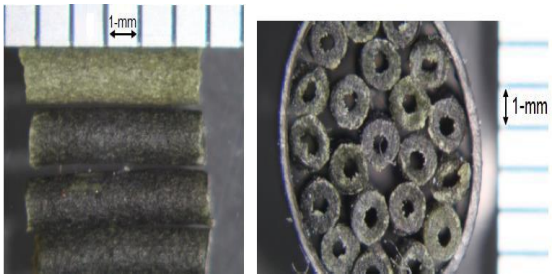

Figure 7. Photographs of M1 Propellant Showing Tests 1 & 2: Single Perforation (1P) OD: 1.22 m; L: 5.03 mm; Perf: 0.514 mm.

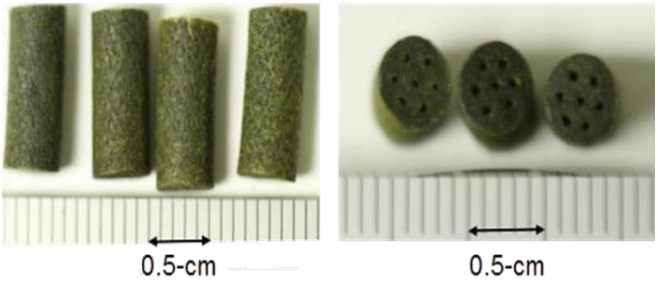

Figure 8. Photographs of M1 Propellant Showing Seven Perforation (7P) Tests 3-7: Seven Perforation (7P) OD: 4.77 mm L: 10.765 mm; Perf: 0.451 mm; Longer mass regression rate; longer burn time.

Table 4. HD 1.3 China Lake Test Summary.

Test Number	Grain Type	Propellant Weight (kg)	Loading Density (g/cm^3)	Number of Barrels	Structural Failure Observed
1	1P	134.55	0.017	3	No
2	1P	534.55	0.067	8	Yes
3	7P	120.00	0.015	3	No
4	7P	503.64	0.063	8	Yes
5	7P	120.00	0.015	3	No
6	7P	534.82	0.063	7	Yes
7	7P	240.55	0.030	3	Yes

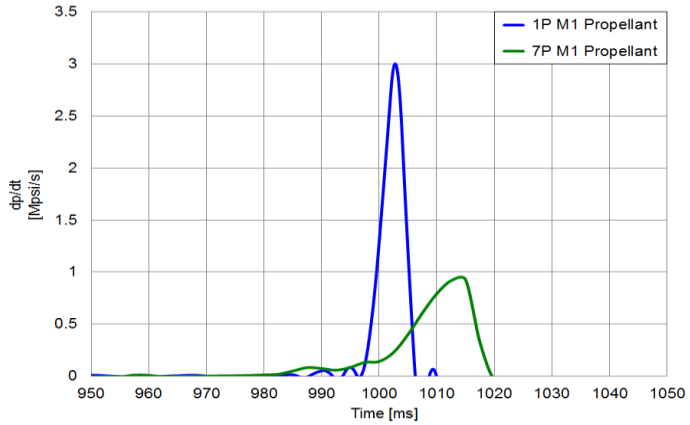

Figure 9. Pressurization Rate Versus Time for Two M1 Propellant Geometries [5,6,8].

Structural Effects (Confinement / Environment)

Unchoked condition is achieved when there is enough venting of the structure such that the structure never builds up very much pressure. Choked flow condition, on the other hand, is achieved once the internal pressure is about two times that of the external pressure, then the pressure rises very quickly and quickly ruptures the structure. Unchoked flow there is no significant pressure build up inside the structure versus chocked flow there is significant pressure buildup inside the structure.

Since the current siting criteria for HD 1.3 is based on fireball radius as previously discussed, the ESSD or QD in the DODM 6055.09-M [1] do not account for effects such as structural lethal debris, pressurization effects, and potentially directional heat flux effects. Structures may pressurize and fail when the internal pressure exceeds two times that of the external pressure. Pressurization is a competition between the pressure produced from the burning of the energetic system (exothermic-depending on the type of material may produce significant concentration of gas by-products) and venting of the structure. The pressurization due to reaction from solid energetic material to product gases is dependent on the density of the solid, the surface regression rate of the solid (often called the linear burning rate), the burning surface area, and the thermochemistry of the reaction. Because gun propellants have high surface area available for combustion, they produce rapid pressurization. Choked flow occurs when the

pressure inside a vessel or structure exceeds the ability to vent. Once the flow is choked, pressure inside the structure can increase rapidly as the energetic material burns inside the structure thus creating a significant structural debris hazard not currently accounted for in the DODM 6055.09 QD [1] tables for HD 1.3 systems.

The non-dimensional vent area ratio (VAR) is a term used to describe venting (Equation 3).

$$VAR = A_v / (V_{ch})^{2/3} \tag{3}$$

where A_v refers to the surface area of the vent, and V_{ch} describes the volume of the chamber.

The *loading density* of energetic material is defined as the weight of energetic material divided by the volume of the structure. A high VAR and a relatively low loading density are needed for a structure to survive pressurization. Figure 10 is a plot of the VAR versus the loading density for the tests of Table 4 and several tests described in Allain [14] and Herrera et al. [15]. The tests at an M1 loading density greater than 0.03 g/cm^3 resulted in rupture of the structure and, thus, choked flow, while those with less than 0.03 g/cm^3 where the structure survived were unchoked.

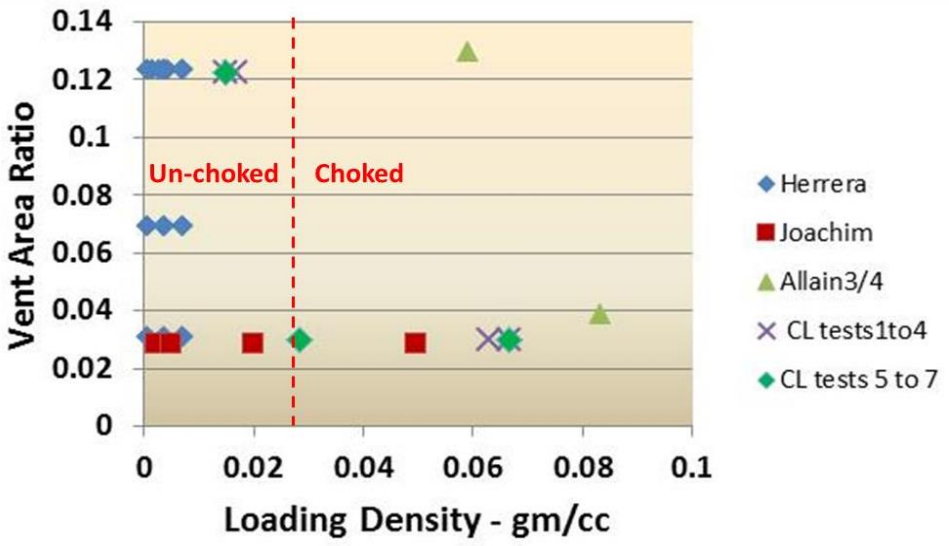

Figure 10. VAR Versus Loading Density for M1 Subscale Testing.

The concrete of the structure walls in all of the tests were color-coded in order to identify the fragment source. External high-speed digital video, Doppler velocimetry, and infrared camera coverage were also included. The tests were internally and externally instrumented using pressure, temperature, and heat flux gauges. The individual 360-degree fragment mapping was documented for the tests that resulted in structural failure.

Table 5 summarizes the pressure data and combustion results from all seven tests. Table 6 summarizes the structural debris (secondary fragments) from all seven tests. The discussions that follow attempt to correlate these results to hazards associated with HD 1.3 system and present some initial improvements to the QD (or ESSD) data currently in DODM 6055.09-M [1].

Table 5. Summary of Pressure Data and Combustion Results From Seven Tests.

Test Number	Max P_{in} (MPa)	Max P_{out} (MPa)	Max T_{in} (C)	Max T_{out} (C)	Max Hf_{in} (kW/m^2)	Max Hf_{in} (kW/m^2)
1	0.0139 (36.98 s)	0.011 (93.11 s, 50 m)	~753 (52.78 s)	971 (6.9 s, 5 m)	1835.44 (38.50 s)	4347 (6/5 s. 5 m)
2	0.368 (1.40 s)	0.236[a] (1.4 s, 10 m)	1101.85 (10.82 s)	164.66 (1.5 s, 10 m)	158.22 (11.38 s)	900 (5 m)
3	0.008 (10.4 s)	< 0.007	1118.71 (15.7 s)	855	171.68 (11.55 s)	15027.93 (13.5 s)
4	0.234 (2.27 s)	0.012	1250[c]	101.45 (1.5 s, 10 m)	210.63 (11.5 s)	1137.89 (13.5 s, 3 m)
5	0.033 (5.31 s)	< 0.007	1250[c]	1250*** (7.5 s, 13 m)	62.58 (9.5 s)	1942.93 (17.5 s, 5 m)
6	0.446 (2.79 s)	0.026 (2.82 s, 11 m)	1250[c]	322.55 (30.09 s, 5 m)	13000 (3.75 s)	1137.89 (13.5 s, 3 m)
7	0.366 (8.04 s)	0.014 (8.02 s)	1250[c]	595.3 (19.32 s)	179.99 (9.25 s)	1642.93 (17.5 s, 5 m)

[a]Pressure value might have been caused by a fragment impacting the sensor. All other pressure values for this test were <1 psi.

[b]Value recorded after structural failure.

[c]Thermocouple upper limit.

Table 6. Summary of Structural Debris (Secondary Fragment) for Tests That Resulted in Structural Failure.

Test Number	Total Collected	Total Outside IBD	Heaviest	Furthest
2	2,609	2,177	8.4 kg (37m)	105 m (76 g)
4	3,244	1,458	11.5 kg (31.5)	156 m (23.7 g)
6	3,415	546	19.01 kg (19.03 m)	128 m (168 g)
6	778	293	3.48 kg (15 m)	

The effect of surface area on the maximum internal pressure versus time is seen for Tests 2 and 4 in Figure 11. The maximum pressure is higher for the 1P propellant with the higher surface area and reaches peak pressure about 1 second earlier than the 7P test.

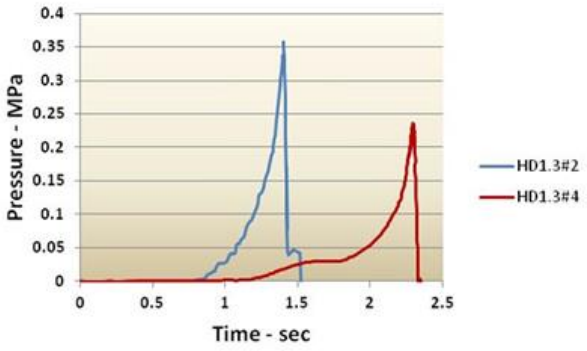

Figure 11. Surface Area Comparison for Tests 2 and 4.

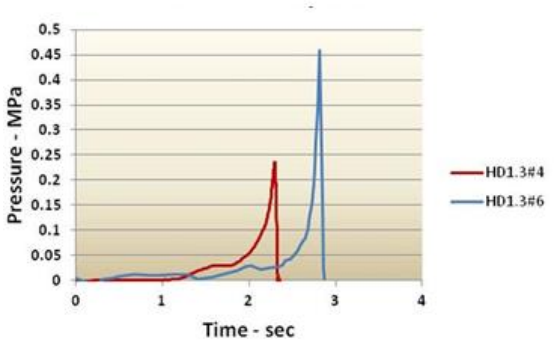

Figure 12. Structural Comparison for Tests 4 and 6.

The effect of increasing the structural strength is illustrated in Figure 12 in the plot of the maximum internal pressure of Tests 4 and 6. The structure of Test 6 held the pressure about 0.5 second longer and reached a pressure nearly two times that of Test 4.

The effects of loading density can be seen in the maximum internal pressure plots of Tests 6 and 7 in Figure 13. The lower loading density of Test 7 resulted in a longer ignition delay and lower pressure, likely due to increased heat loss.

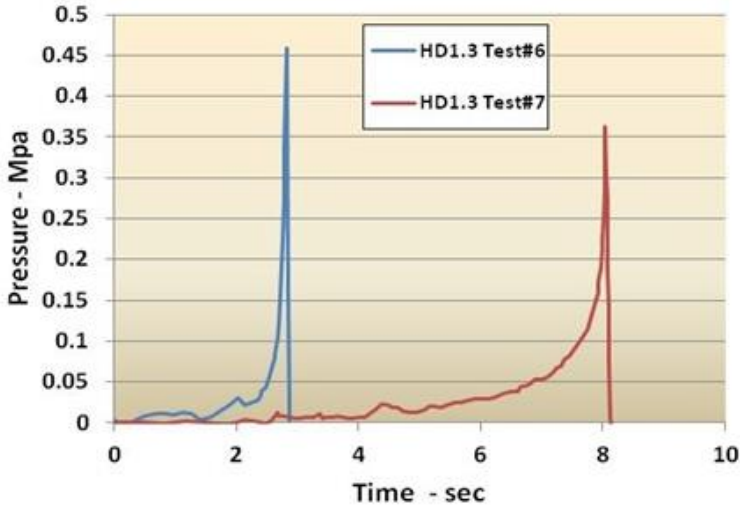

Figure 13. Loading Density Comparison.

Plume and fireball formation for Test 4 are illustrated in Figures 14 and 15, respectively.

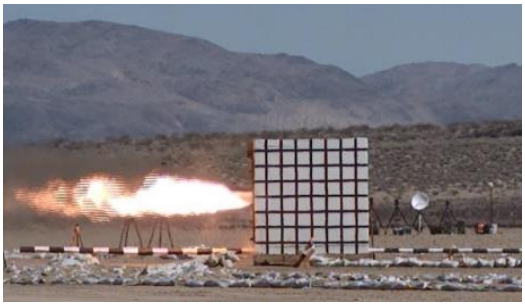

Figure 14. Kasun Structure Illustration of Plume Still Photograph From High-speed Video, Test 4.

Figure 15. Illustration of Fireball, Still Photograph From High-Speed Video, Test 4.

A comparison of the maximum temperature measured externally in alignment with the orifice of the structure for Tests 2 and 4 is given in Figure 16. Maximum temperatures were slightly lower for Test 4 than for Test 2. These differences may be related to the prevailing wind conditions as these temperatures were measured externally after structure failure. A maximum thermal flux measured in the fireball after the structure failed was 158.22 kW/m^2 and 210.626 kW/m^2 for Tests 2 and 4, respectively.

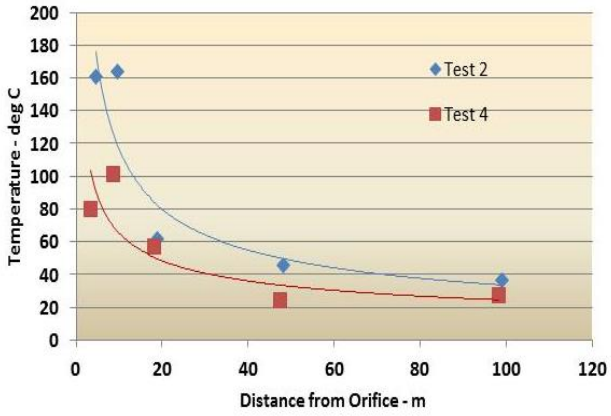

Figure 16. Maximum Temperature Measured at Distance in Alignment With Structure Orifice.

A plot of peak heat flux measured with respect to the exit plume of Test 5 (no structural failure) is given in Figure 17. The IBD calculated for this test is given by the dashed green line.

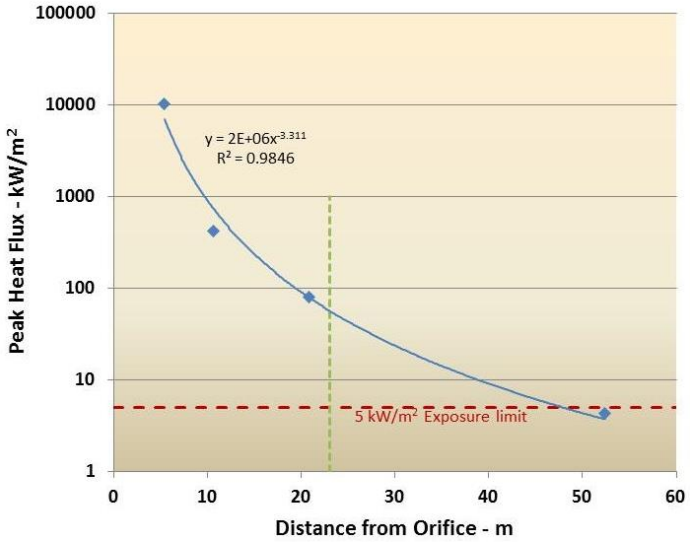

Figure 17. External Plume Heat Flux Measurements for Test 5.

The reactions observed in the high-speed video can be related to the pressurization curves and are illustrated for Test 4 in Figures 18 and 19. The initial pressurization is related to the first light/gasification of the M1 propellant as seen by the illuminated orifice in Figure 18 (first blue arrow), at the initial pressure rise followed by complete ignition (fully illuminated orifice in Figure 18 (second blue arrow). A small flamelet can be seen exiting the structure at the complete ignition time in the orthogonal view of the structure. The later time events of plume formation and failure of the structure are illustrated in Figure 19. Fireball formation and debris throw occurred at the time indicated by the asterisk in Figure 19. The structure failed at the roofline in both Tests 2 and 4.

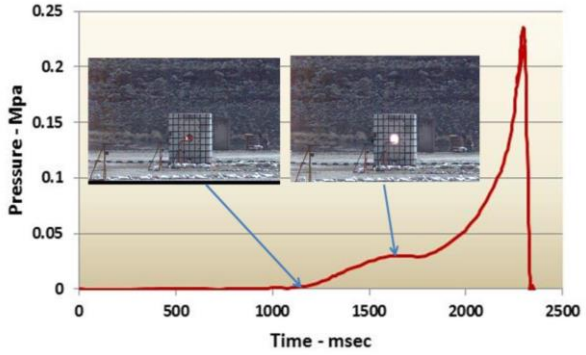

Figure 18. Relating the Plume/Fireball Formation With Internal Pressure, Test 4.

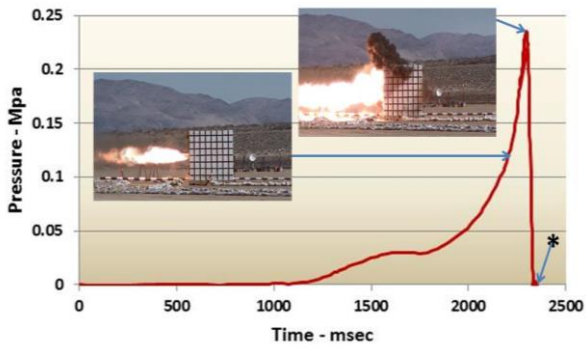

Figure 19. Plume Formation and Structural Failure, Test 4.

Table 7 is a summary of current magazine structures, maximum loading density, and assessing the VAR. In all cases if these magazines had an NEW of 500,000 lbs (226,796 kg) the magazines would result in a choked flow condition.

Table 7. Magazine Type With Corresponding Loading Density and VAR.

Magazine Type and Dimensions	Maximum Loading Density Assuming 226796 kg NEW (g/cm^3)	VAR $A/V^{2/3}$
RC Box 421-80-06	0.364	0.316
RC Circular Arc, NAVFAC 1404310-1404324		
24.38 m long, door area 9.29 m^2	0.43	0.1423
24.38 m long, door area 14.86 m^2	0.43	0.228
RC Arch 421-80-05		
27.43 m long, door area 5.95 m^2	0.3	0.0725
27.43 m long, door area 9.29 m^2	0.3	0.113
24.38 m long, door area 5.95 m^2	0.338	0.0785
24.38 m long, door area 5.95 m^2	0.338	0.122
18.29 m long, door area 5.95 m^2	0.45	0.0951
18.29 m long, door area 9.29 m^2	0.45	0.148
Steel Arch 421-80-01		
27.13 m long, door area 5.95 m^2	0.309	0.073
27.13 m long, door area 9.29 m^2	0.309	0.114
Lone Star, 18.29 m x 8.08 m x 3.89 m	0.252	0.0691
Indian Head, 24.99 m x 7.62 m x 3.35 m	0.226	0.0691
Radford, 25.04 m x 7.62 m x 3.96 m	0.191	0.0299

Structural Debris (Secondary Fragmentation) Patterns

The structural debris data are summarized in Table 8 for Tests 2, 4, 6, and 7. Tests 2 and 4 addressed the differences of configuration/geometry of the M1 grains. Tests 4 and 6 addressed structural differences. Lastly, Tests 6 and 7 addressed loading density.

Table 8. Summary of Structural Debris Map Data for All the Tests That Exhibited a Chocked Flow Condition.

Test Number	Total Fragments Collected	Total Fragments Found Outside IBD	Heaviest Fragment	Furthest Fragment
2	2,609	2,177	8.4 kg (37m)	105 m (76 g)
4	3,244	1,458	11.5 kg (31.5)	156 m (23.7 g)
6	3,415	546	19.01 kg (19.03 m)	128 m (168 g)
6	778	293	3.48 kg (15 m)	

The fragment map of Test 2 is given in Figure 20, where the circles indicate distance from the original structure; orange at 4.6 meters (15 feet), yellow at 15.2 meters (50 feet), red at 30.5 meters (100 feet) and brown at 76.2 meters (250 feet). Over 2,609 debris samples were weighed; their color recorded, and their location mapped. The Test 2 fragment map shows that most of the fragments were from the roof (black concrete). Fragments weighing less than 5 grams were not recorded in any of the HD 1.3 tests. Additionally, in Test 2, some of the fragments weighing less than 200 grams were not collected in the southern and western areas of the site within the 21.3-meter (70-foot) radius from the center of the original structure due adverse weather conditions. The furthest recovered fragment of Test 2 was from the north quadrant at 105 meters (341 feet) from the center of the structure and weighed 76 grams. The heaviest recovered fragment was found 37 meters (121.4 feet) from the structure and weighed 8,400 grams. The calculated IBD, or public traffic route distance (PTRD), for this test was 23.3 meters (76.41 feet), and the calculated inter-magazine distance (IMD), or ILD, was calculated to be 15.798 meters (51.83 feet) [6]. Numerous fragments landed beyond the calculated IBD/PTRD.

The fragment map for Test 4 is presented in Figure 21. The origin of the map is the center of the structure. This test produced fragments from all side walls and roof. The farthest fragment measured was 156 meters (512 feet) from the origin and was identified as part of the roof. The IBD calculated for this test was of 23 meters (75 feet). A vast amount of fragments landed beyond this boundary. The largest fragment collected weighed 11,555 grams, and it landed 31.5 meters (103 feet) from the origin. According to the color of the fragment, it was determined it came off of the roof. This fragment, along with 1,419 of the 3,245 fragments recovered, landed beyond the IBD. The fragment data from these two tests indicate that the slower reacting 7P propellant with the lower surface area produced a larger number fragments beyond the calculated IBD than did the 1P, Test 2.

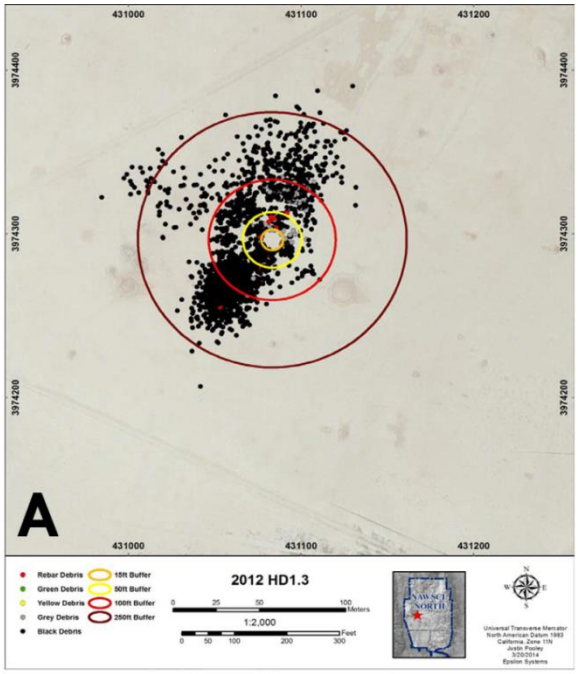

Figure 20. Fragment Map of China Lake Test 2.

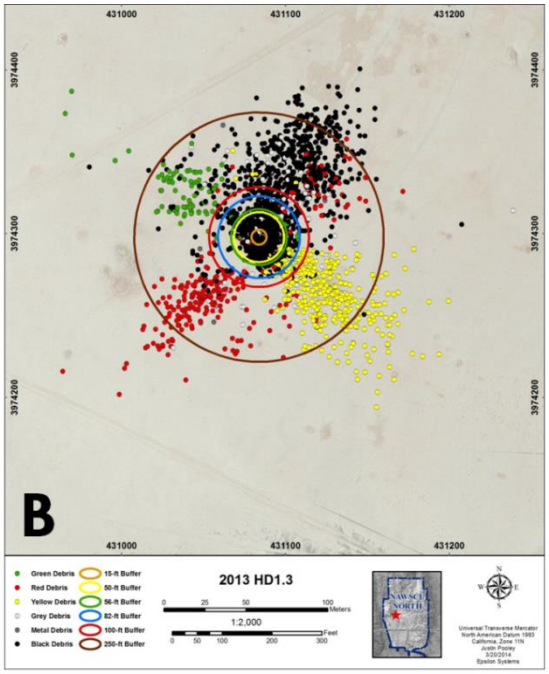

Figure 21. Fragment Map of China Lake Test 4.

Fragment maps and a still picture taken from the video for Tests 4 and 6 are compared side-by-side in Figures 22 and 23. The Kasun structure in these two tests varied in the degree of reinforcement in the corners. The Test 6 structure had significantly more steel reinforcement. Data collected from the high-speed images and the fragment mapping indicate that initial structural failure occurred at the roof and walls in Test 4, whereas the structure used for Test 6 primarily failed at the floor. The weak points in each of the structures influenced the trajectory of the structural debris. The orange, yellow, red, and brown circles are at the 4.6 meters (15 feet), 15.2 meters (50 feet), 30.5 meters (100 feet), and 76.2 meters (250 feet) from the structure. The green circle is at 17.1 meters (56 feet), and the blue circle is at 25.0 meters (82 feet).

Data collected from the high-speed images and the fragment mapping indicate that initial structural failure occurred at the roof and walls in Test 4, whereas the structure used for Test 6 primarily failed at the floor. The weak points in each of the structures influenced the trajectory of the fragment flight. Fragment maps and a still picture taken from the video for Tests 4 and 6 are compared side-by-side in Figures 22 and 23 and summarized in Table 3. The green circle is at 17.1 meters (56 feet), and the blue circle is at 25.0 meters (82 feet) and represents (IBD.

There were 3,245 and 3,415 fragments collected in Tests 4 and 6, respectively. About 44% of the collected fragments in Test 4 were outside of IBD as compared to about 16% in Test 6. This difference is probably due to the direction of the fragment flight path in the two tests as a result of the changes in structure construction.

Fragment maps and a still picture taken from the video for Tests 6 and 7 are compared side-by-side in Figures 24 and 25. These data demonstrate the effect of loading density on structural debris formation.

The importance of reinforcement configuration at the wall and roof interfaces was illustrated when comparing the results obtained for Tests 4 and 6. The modifications to the rebar reinforcement used in Tests 6 and 7 could have caused the structures to withstand the internal pressure for a longer period of time, increasing the time to failure, and allowing for higher internal pressures to be generated. All tests failed well below the calculated theoretical pressure. Unburned propellant grains were recovered in at least one test (Test 6).

The failure location observed in all tests influenced the directionality and amount of fragments that landed outside of IBD. Test 4 failed at the roof while Test 6 failed at or near the floor. The fragment trajectory tended to be directed into the ground in the latter case. The failure at the roof experienced by the structure in Test 4 generated a much larger percentage of small fragments (5 to 15 grams) and, although most fragments came from the roof, the walls of this structure were also fragmented. The fragment maps indicate that the added concrete reinforcement in Test 6 helped the structure to survive for longer and reduced the number of fragments projected outside of the IBD. Nevertheless, Test 6 still had 546 fragments landing outside IBD.

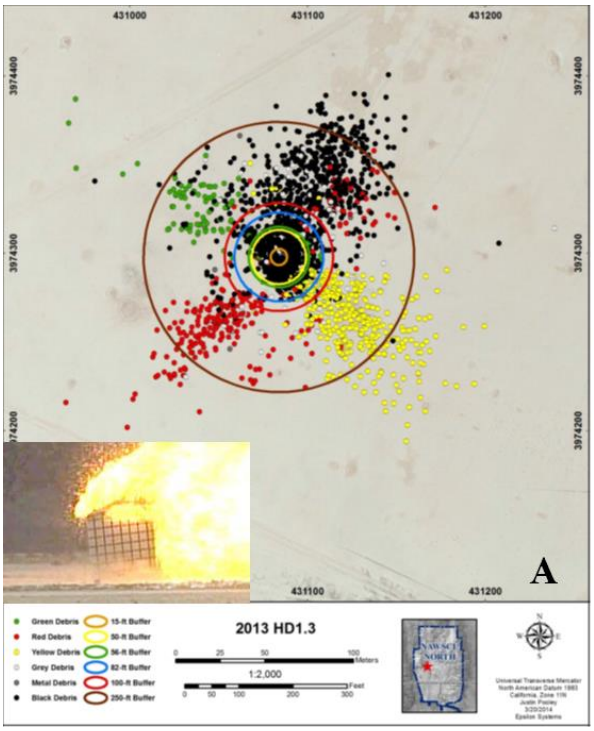

Figure 22. China Lake Test 4 Fragment Map and Structural Failure.

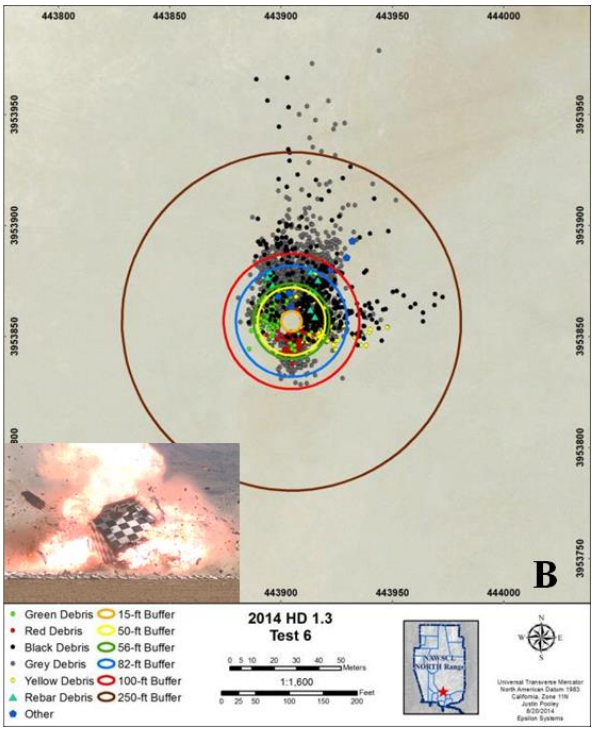

Figure 23. China Lake Test 6 Fragment Map and Structural Failure.

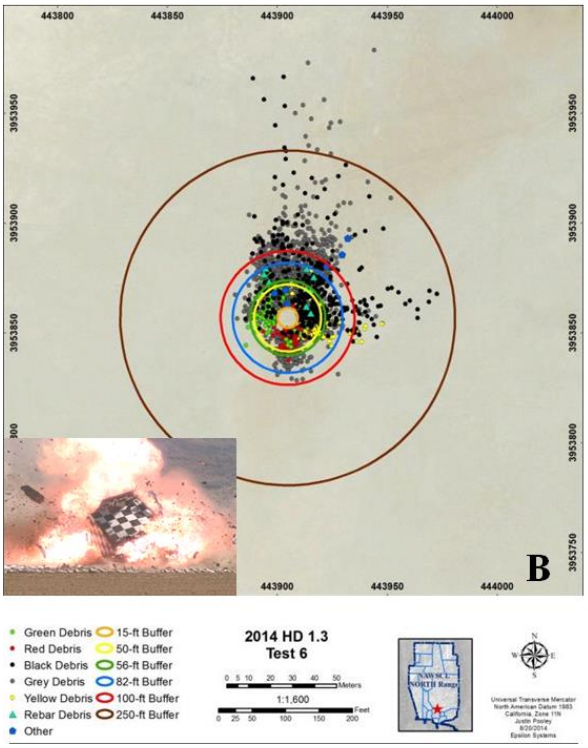

Figure 24. Fragment Map of China Lake Test 6.

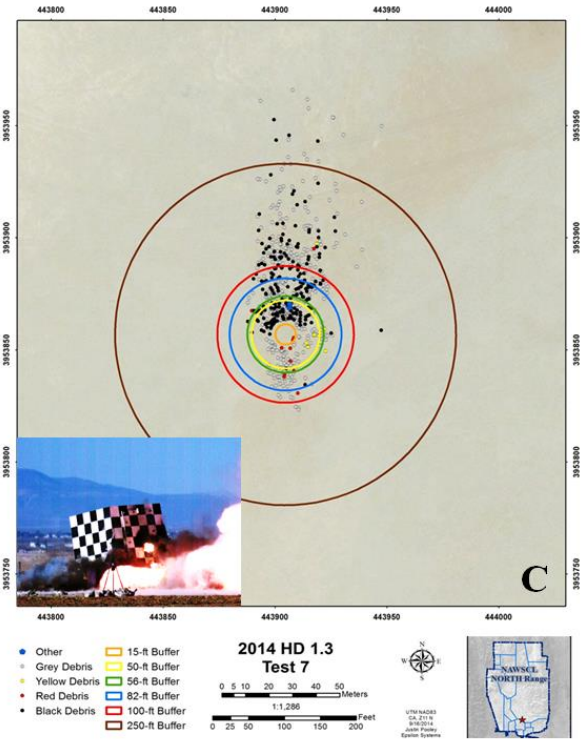

Figure 25. Fragment Map of China Lake Test 7.

Directional Thermal Effects From the Subscale Tests

Romo et al. [8] provides a detailed discussion of the thermal effects of classes of propellants. Decay in external temperatures was observed for Tests 4, 6, and 7 as the distance from the structure increased. The external maximum temperatures recorded for Test 6 were higher than those of Test 4. These results could have been

influenced by several factors, including the early structural failure observed in Test 4 and the prevailing winds changing the directionality of the fire plume. The differences observed between maximum external temperatures for Tests 6 and 7 could have been influenced by the directionality of the plume and the internal placement of the fiber barrels containing the M1 propellant relative to the orifice. External maximum temperatures, coupled with heat flux data presented in References [7] and [8], showed that the thermal hazard at IBD was considerable for all three tests.

A general observation that can be made between the two sets of tests is relative to the different time regimes that exist between a shock-driven versus a combustion-driven hazard event. There are two orders of magnitude difference in the time response between the pressure versus time of the HD 1.1 and Tests 2 and 4 of the HD 1.3 tests, shown in Figure 26. The longer, slower pressurization will result in larger fragments, many of a flat, plate-like shape resulting in longer distance projection relative to their mass. Thermochemistry, heat loss as well as venting will contribute to the pressure differences between the combustion and detonation-driven tests.

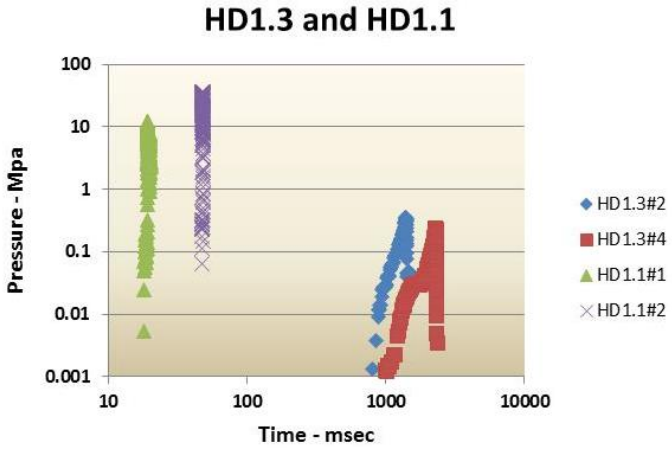

Figure 26. Time Difference Between Prompt Shock and Combustion-Driven Events.

The importance of reinforcement configuration at the wall and roof interfaces was illustrated when comparing the results obtained for Tests 4 and 6. The modifications to the rebar reinforcement used in Tests 6 and 7 could have caused the structures to withstand the internal pressure for a longer period of time, increasing the time to failure and allowing for higher internal pressures to be generated. All tests failed well below the calculated theoretical pressure. Unburned propellant grains were recovered in at least one test (Test 6).

The failure location observed in all tests influenced the directionality and amount of fragments that landed outside of IBD. Test 4 failed at the roof while Test 6 failed at or near the floor. The fragment trajectory tended to be directed into the ground in the latter case. The failure at the roof experienced by the structure in Test 4 generated a much larger percentage of small fragments (5 to 15 grams) and, although most fragments came from the roof, the walls of this structure were also fragmented. The fragment maps indicate that the added concrete reinforcement in Test 6 helped the structure to survive for longer and reduced the number of fragments projected outside of the IBD. Nevertheless, Test 6 still had 546 fragments landing outside IBD.

The HD 1.3 tests with the HD 1.1 tests described in Berglund et al. [19] and Gronsten et al. [17]; however, referring back to the simplified risk/hazard model Figure 1, it became apparent that there are too many variables to permit a direct comparison of the results. The HD 1.1 tests were initiated by a detonation (prompt shock), while the HD 1.3 tests were initiated by combustion (electrical ignition). Secondly, there was no venting of the Kasun structure in the HD 1.1 tests. A general observation that can be made between the two sets of tests is relative to the different time regimes that exist between a shock-driven versus a combustion-driven hazard event. There are two orders of magnitude difference in the time response between the pressure versus time of the HD 1.1 and Tests 2 and 4 of the HD 1.3 tests, shown in Figure 26. The longer, slower pressurization will result in larger fragments, many of a flat, plate-like shape resulting in longer distance projection relative to their mass. Thermochemistry, heat loss as well as venting will contribute to the pressure differences between the combustion and detonation-driven tests.

Proposed Explosives Safety Quantity Distance

The QD tables from DODM 6055.09-M summarized in Figure 27 contain data from the M1 tests that exhibited structural failure. The data plotted are the furthest structural debris (secondary fragment) recovered from each test. The figure also includes data from a few mishaps were debris was collected.

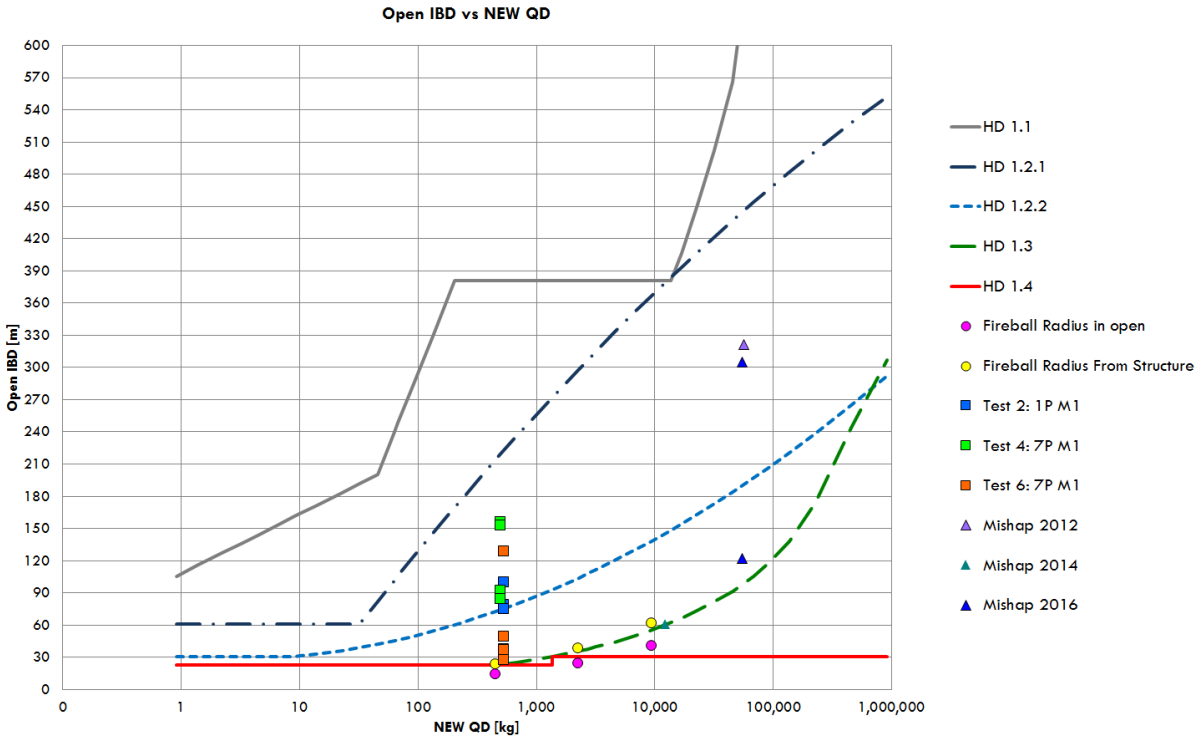

Figure 27. IBD Versus NEW in SI Units Including Fireball Calculations and Debris (Secondary Fragments) From Mishap Data.

Figure 27 is the same IBD data plotted in Figure 2 with the addition of available mishap data and test results. From this figure, one can conclude that the current HD 1.3 table does not account for all the hazards associated with HD 1.3 combustion inside a structure. In all instances, the IBD documented in DODM 6055.09-M [1] and AASTP-1 [2] for HD 1.3 is much less than the test data indicate. The current HD 1.3 IBD is the fireball distance measured from detonation events and not a true representation of the test results. At this fireball, distance any person exposed is expected to be an instantaneous fatality.

In the 2012 update of DODM 6055.09-M, the permissible exposure for accidental ignition or initiation of explosives was changed to reflect the improved thermal requirements. The new manual now states in V1.E9.3 [1]:

> "When required, personnel protection must limit incident blast overpressure to 2.3 psi [15.9 kPa], fragments to energies of less than 58 ft-lbs [79 joules], and thermal fluxes to *prevent the onset of second-degree burns (heat fluxes and exposure times experienced by personnel should be less than that given by the equation t=200q-1.46 where "t" is the time in seconds that a person is exposed and "q" is the received heat flux in kilowatts (kW) per m^2)*".

It should be noted that the values reported in Figure 27 in all cases are at much higher heat flux than required in the DODM 6055.09-M and vary based on the combustion characteristics of the specific energetic as discussed previously in this paper. In all cases, these lines represent the prompt death line and not the line for second-degree burn suggested by the 2012 heat flux update of the DODM 6055.09-M.

Figure 28 graphs the new thermal requirement (solid green line) and compares it to the other QD values. As shown, the new thermal flux (to protect a person from second-degree burns) is significantly higher than the HD 1.3 QD values outlined in the DODM 6055.09-M [1] or AASTP-1 [2]. The new heat flux thermal requirement is also much higher the "slow combustion" and the "detonation and rapid combustion" fireball diameter from Figure 3. This proposed IBD (based on DODM 6055.09-M heat flux allowance, green solid line) does not take into account any directional plume effects seen by the testing. Furthermore, it does not consider the hazards associated with lethal equipment and/or structural debris associated with failure due to chocked flow conditions associated

with combustion effects. However, this new QD curve based on thermal flux and prevention of second-degree burns does bring the hazards effects from combustion-driven evens more in line with the hazards of HD 1.1 and HD1.2.x.

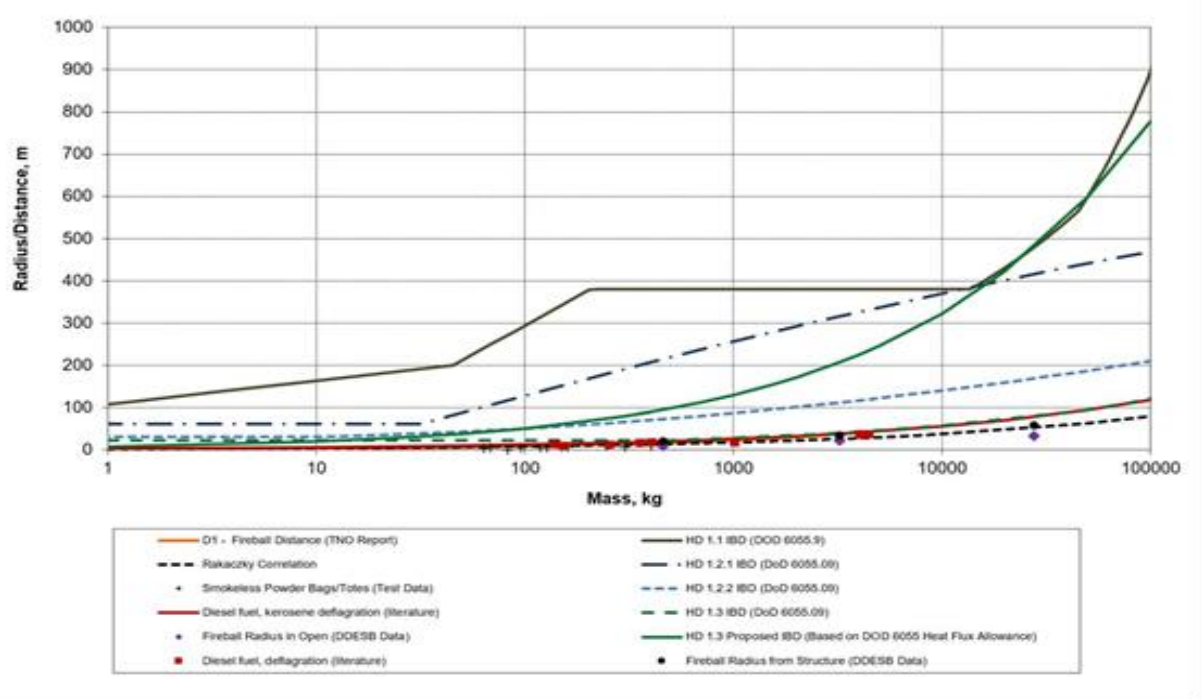

Figure 28. IBD Versus Mass (kg) With 2012 Proposed IBD Based on Heat Flux to Protect Personnel From Second-Degree Burns [1].

Summary/Conclusions

A thermal stimulus either externally applied (fire) or by internal means is most often seen during the munition life cycle and is responsible for over 75% of large mishaps [8]. The chemical composition, physical state, and geometry of the energetic system coupled with the amount of confinement will define severity of the reaction and the resulting effects as controlled by ESSD or QD.

Romo et al. concluded that basic combustion properties of the HD 1.3 item or bulk substance drive the ease of ignition and subsequent combustion behavior [7]. The ease of ignition by thermal stimulus at low pressure is critical with respect to handling safety. Most of the HD 1.3 ammonium perchlorate (AP)-based propellants readily ignite and burn at ambient pressure, while many HD 1.1 nitramine-based explosives are difficult to ignite at relatively low pressures. In contrast, the nitramine-based HD 1.1 formulations often readily gasify without complete ignition, generating reactive gaseous products that can then contribute to convective burning and deflagration-to-detonation transition (DDT). Within a family of energetic materials, the higher the burning rate the shorter the time to complete ignition.

Furthermore, Romo et al. recommended that burning rate measurements should be extended beyond the range of operational design for understanding hazards response [7]. Low-pressure burning rate measurements provide insight into the ease of ignition and potential for extinguishment in a formulation. These data are useful in describing the hazards potential in both handling and storage. The materials that burn well at ambient pressure generally are also the easiest to ignite, making them the most vulnerable in a thermally induced transportation and storage incident. High-pressure burning rates provide insight into the stability of the burning grain and rate of pressurization. The rate of pressurization relative to the rate of depressurization or venting is critical in the level of reaction violence in a storage situation. The available surface area of an energetic material, either HD 1.1 or 1.3, has an effect on the mass regression rate as well. The higher the available surface area of the energetic, either by manufacture or damage, the higher the mass regression rate of the substance will be. Reaction violence will likely increase as well.

In summary, HD 1.3 Test 2 versus Test 4 addresses differences in propellant surface area. HD 1.3 Test 4 versus Test 6 addresses the structural differences. HD 1.3 Test 6 versus Test 7 addresses the difference loading densities. Both Tests 2 and 4 exhibited choked flow resulting in the failure of the structure. The difference in propellant

surface area (small, 1P versus large, 7P grains) was evident in the pressurization and rupture of the structures. The structure containing the higher surface area 1P grain rupture occurred at 1.4 seconds, while the lower surface area 7P grain occurred at 2.3 seconds. The structure failed at the roof in both tests. Plume and subsequent fireball formation were directional with the majority of structural fragment debris originating from the roof of the structure. Structural debris was recovered at distances beyond the IBD calculated for the M1 loading density of these tests. The slower reacting 7P sample appeared to produce more fragments beyond the calculated IBD than the higher surface area 1P sample; however, further testing is needed to validate this observation. Secondly, from HD 1.3 Tests 4 and Test 6 all the data, time to structural failure, and debris map indicate that the more robust structure held together longer and produced fewer secondary fragment (less structural debris). The loading density differences between Tests 6 and Test 7 were consistent with the lower loading density having a lower pressure build up, structure failed at a later time, and the debris map had fewer secondary fragment (less structural debris).

Addressing the question of unchoked flow (no rupture) or choked flow (rupture with projection of structural debris), if a person was directly in the plume or fireball even in these relatively small tests, they would have quickly become a fatality due to the high temperatures of the exit plume. Even if a person was not directly in the plume or fireball, the radiation hazard in terms of heat flux and exposure time might still result in fatalities. A thermal flux of 10 kW/m^2, for example, will result in second-degree burns at 6.9 seconds exposure time, while a heat flux of 15 kW/m^2 will cause second-degree burns at 3.8 seconds exposure time. A flux of 5 kW/m^2 gives 19.1 seconds before the onset of second-degree burns, giving a modest amount of time to recognize the threat and take evasive action. The petroleum industry uses a criterion of 5 kW/m^2 at the boundary fence as one of their safety criterion for fire in refineries [18]. Fortunately, the heat flux diminishes roughly as $1/d^2$ with d being the distance from the plume or fireball. Even more important, any barrier (such as another structure, car, thermal blanket, etc.) can significantly reduce the thermal flux. World War II (WWII) vintage magazines were constructed using a frangible headwall with a barricade some distance away from the headwall. These designs warrant reinvestigation and possible reconsideration for future designs.

Tests 2, 4, 6, and 7 resulted in large directional plumes followed by a fireball upon structural failure. Calculated fireball diameters of 27 meters (88 feet) in Test 2, 26 meters (86 feet) in Test 4, 39 meters (128 feet) in Test 6, and 41 meters (136 feet) in Test 7 from DODM 6055.09-M [1] were surpassed in all tests. Temperature and thermal flux measurements indicate a thermal hazard beyond the current regulatory descriptors. These studies are being used to improve the phenomena and descriptors relative to the HD 1.3 events; however, much more testing is warranted to ensure that the ESSD or QD tables can be improved by considering directional thermal effects, fireball, structural failure, and structural debris.

Initial modification of the ESSD or QD table to account for second-degree burn proposed shows that for the most part the HD 1.3 IBD increases significantly as the total mass increases. This does not take into account directional effect from either the structure or the plume as illustrated for the directional plume in Test 5. It does not take into account the structural breakup occurring when choked flow conditions exist inside the structure.

Future Efforts

The studies summarized in this paper serve to highlight a number of areas where more data and models are needed. The HD 1.3 category is very broad and studies are needed for more than a single substance type and/or item. The M1 propellant tested in the subscale tests is not the most energetic of the bulk gun propellants that might be found in a storage or transportation environment. A further complication is that in the U.S., mixed storage is common; for example, an all-up round (AUR) might be composed of an HD 1.1 warhead, an HD 1.3 rocket motor, and numerous HD 1.4 auxiliary items. The AUR will be stored at the highest hazard designator, HD 1.1, but contain substances at hazard levels that are more sensitive to a thermal stimulus than the HD 1.1 explosive fill. Also, the components may have an "estimated TNT equivalent" weight that is much less than the actual energetic mass. This equivalent weight is what is summed as part of the total NEWQD or maximum credible event (MCE) weight.

Ignition and burning rate measurements are commonly performed on solid rocket propellant for performance purposes, but these measurements are rarely performed on explosives and pyrotechnics. The energetic fills used in HD 1.1, HD 1.2.x, HD 1.3, and HD 1.4 items should be well characterized. Measurements at pressures above and below the operating regime of the systems are also rare but should be considered for evaluation of the hazard threat. Low-pressure burning rates of gun propellants are of particular interest. These measurements should not be made for measurement sake but should be based on the critical hazards identified in a threat hazards assessment or the parameters needed in model development improvement and function.

Confinement scenarios that closely simulate those found in transportation and storage need to be investigated. Light confinement of shipping containers as well as the heavy confinement found in an earth-covered magazine

should be studied. The 2 m^2 concrete structure, while large in comparison to the laboratory tests, is relatively small when compared to many storage magazines, and scaling factors are unknown. The loading density used in the HD 1.3 subscale tests was aimed at identification of the differences between choked and unchoked venting and did not address the average magazine loading densities that are often much higher than those in the 2 m x 2 m x 2 m structures. Packing arrangements and loading density should be studied to gain a better understanding of the flame spreading ability within the confining environment in addition to the contribution of dunnage to the combustion-driven event. In some instances, the program may wish to consider storing combustible systems in lightweight structures or structures with frangible walls.

Significant considerations need to be made when siting facilities meant to use or store energetic materials. This requires many tests and time before coming up with a satisfactory solution. The DDESB is collaborating with government and industry agencies to develop test programs, enhance structural designs, and develop modeling tools in order to achieve appropriate solutions. These capabilities will use design of experiments approaches and parametric modeling efforts in order to determine critical factors driving the determination of ESSD or QD for all hazards. The outcome of these efforts should take into account aspects of risk management, process safety management, and hazards identification/mitigation [20]. The approach should be based on the understanding that a single siting procedure may not be appropriate, as demonstrated by the structural requirements for mitigation of a detonation-type reaction versus a combustion reaction are contradictory. For example, one of the mitigation approaches for a detonation reaction is the use of robust concrete structures, while significant venting, frangible panels, and light frame/confinement are required to mitigate hazards for a combustion-type reaction. Balancing these opposing design constraints in one facility will require a lot of technical and engineering work, as well as collaboration across various backgrounds and fields of study.

A step-by-step risk assessment and hazard identification is required for all the operations that are performed in explosives facilities. Considerations of thermal hazard, choked vs unchoked conditions, directional effects, lethal structural and instrumentation debris, impulse and blast as a function of time need to be evaluated in siting of all facilities. Thus, the explosives safety community is encouraged to begin exploring siting by hazards to allow for more comprehensive assessments of all operational, processes, and materials hazards. Moving towards reaction hazards siting will enable program developers to think about the balance between performance, safety, and costs and make comprehensive risk-management decisions during all stages of the program life cycle.

Acknowledgements
The authors would like to acknowledge Dr. Clint Guymon from the Safety Management Services, Inc. for many technical exchanges and contribution to the modified heat flux data based on the 2012 change to the DODM 6055.09-M.

References

1. Office of the Deputy Under Secretary of Defense (Installations and Environment), "DOD Ammunition and Explosives Safety Standards," DODM 6055.09-M, Volumes 1-8 date varies by volume, Washington, D.C. (2008). Vol.1, Enclosure 8 and 9 were updated in 2012.
2. AASTP-1, NATO Guidelines for the Storage of Military Ammunition and Explosives, Edition B, Version 1, December 2015.
3. M.M. van der Voort, E. Deschambault, J.A.J. de Roos, T.N. Taylor, "Experimental and Theoretical Basis of Current NATO Standards for Safe Storage of Ammunition and Explosives" P187 MABS 2016.
4. T. L. Boggs, K. P. Ford, and J. Covino, "Realistic Safe-Separation Distance Determination for Mass Fire Hazards," NAWCWD TM 8668, Naval Air Warfare Center Weapons Division (2013).
5. A. D. Farmer, K. P. Ford, J. Covino, T. L. Boggs, and A. I. Atwood, "Combustion of Hazard Division 1.3 M1 Gun Propellant in a Reinforced Concrete Structure," NAWCWD TM 8742, Naval Air Warfare Center Weapons Division (2015).
6. A. D. Farmer, K. P. Ford, J. Covino, T. L. Boggs, and A. I. Atwood, "Combustion of Hazard Division 1.3 M1 Gun Propellant in a Reinforced Concrete Structure, Part II," NAWCWD TM 8764, Naval Air Warfare Center Weapons Division (2017).
7. DDESB Technical Paper 23-Department of Defense Explosives Safety Board Munition Risk Management (ESMRM)—*Acquisition Lifecycle Considerations, Risk Assessment Process Framework and Associated Tools* (Current edition)
8. C. P. Romo, K. P. Ford, A. D. Farmer, A. I. Atwood, T. L. Boggs, and J. Covino, "The Influence of Combustion Properties on the Hazards Potential of Hazard Division (HD) 1.3 Materials," The 6th International Symposium on Energetic Materials and their Applications 6-10 November, 2017, Tohoku University, Sendai, JAPAN; Science and Technology of Energetic Materials, Vol. 79, No. 1 (2018).

9. Public Law (Title 10, Chapter 141, Sub-Section 2389) “The Secretary of Defense shall ensure, to the extent practicable, that insensitive munitions under development of procurement are safe throughout development and fielding when subject to unplanned stimuli.”
10. Department of Defense Ammunition and Explosives Hazard Classification Procedures, TB 700-2 (Army), NAVSEAINST 8020.8C (Navy), TO 11A-1-47 (Air Force), DLAR 8220.1 (Defense Logistics Agency).
11. NFPA 495: Explosive Materials Code current addition.
12. Thermische Wirkunge bwei Pulverabbranden und-detonationen, B 3113-23 Ueberarbeitete Fassur, December 1984. Partial English Translation.
13. A. I. Atwood, “HD1.3 in the U.S. Navy Inventory,” Proc. Department of Defense Explosives Safety Board, Portland, Oregon, July 2010.
14. L. Allain, “Combustion of Gun Propellant in Igloo, Thermal Flux Measurements,” SNPE, NT No. 153/91/-S/TS/NP, 63 pp (1991).
15. W. R. Herrera, L. M. Vargas, P. M. Bowles, F. T. Dodge, and W. E. Baker, “A Study of Fire Hazards from Combustible Ammunition, Effects of Scale and Confinement (Phase II),” Southwest Research Institute, San Antonio, Texas, (1984). Contract MDA903-82-C-0526, SwRI Project 01-7327, 188 pp.
16. L. H. Christensen and S. Skudal, “Test Program with Small ‘Kasun’ Houses,” Norwegian Defence Estates Agency (Forsvarsbygg), Norway. (FoU Rapport nr. 24/2004.)
17. G. A. Gronsten, R. Berglund, A. Carlberg, and R. Forsen, “Break up Tests with Small ‘Ammunition Houses’, Using Cased Charges—Kasun III.” FOI-R-2749-SE, Forsvarsbygg Report 68/2009 (2009).
18. Society of Fire Prevention Engineers, “Engineering Guide: Predicting 1st and 2nd Degree Skin Burns From Thermal Radiation,” SFPE, Maryland (2000).
19. R. Berglund, A. Carlberg, R. Forsen, G. A. Gronsten, and H. Langberg, “Break up Tests with Small ‘Ammunition Houses,’” FOI, Forsvarsbygg, FOI-R-2202-SE, ISSN 1650-1942 (2006).
20. OMB Circular No A-123 2016; DODI 6055.16; 29 CFR 1910; DODI 6055.01 and NFPA 495 2016.